CHAPTER 10

Textile-Based Rectennas

Mohammed Al-Husseini[1], Abdullah Haskou[2], Nadeen Rishani[3] & Karim Y. Kabalan[3]
[1]*Beirut Research and Innovation Center, Lebanese Center for Studies and Research, Beirut, Lebanon.*
[2]*IETR UMR CNRS 6164, University of Rennes 1, Rennes, France.*
[3]*Electrical and Computer Engineering Department, American University of Beirut, Beirut, Lebanon.*

Abstract

The proliferation of portable devices, their growing integration into human lives and the surrounding environment, and the necessity to keep them powered have led to the increasing interest in radio frequency (RF) energy harvesting and its use in wireless mobile devices charging. The appealing features of flexible and wearable electronics, such as light weight, ease and low cost of fabrication, and the growing attention given to them, have made them a strong candidate for designing circuits like rectennas (rectifying antennas) to scavenge the ambient RF energy emitted by a large number of radio transmitters around us. The obvious advantage of harvesting this type of energy is that it is free and green. This chapter focuses on the design of wearable, and in a more general term, textile-based rectennas. It starts by discussing the electrical characterization of textiles and the methods used to estimate their relative permittivity and loss tangent. It then reviews the most recent wearable antenna designs and their applications, and examines the design and analysis of rectifying circuits used in RF energy scavenging, with focus on their sensitivity and conversion efficiency. The latest rectenna designs are also surveyed.

Keywords: Rectenna, wearable devices, electrical characterization of textiles, rectifying circuits.

1 Introduction

The idea of wireless power transmission started right after the birth of wireless communications. In 1893, Tesla [1] demonstrated the wireless illumination of phosphorescent lamps in his experiments with alternate currents of high potential

WIT Transactions on State of the Art in Science and Engineering, Vol 82, © 2014 WIT Press
www.witpress.com, ISSN 1755-8336 (on-line)
doi:10.2495/978-1-84564-986-9/010

and high frequency. After World War II, the idea of using microwaves to transmit power was researched. In 1964, Brown [2] used a rectenna to power a miniature helicopter. Since then, extensive research has been done to design high-performance rectennas [3–5].

The ambient RF energy is emitted by a large number of different radio transmitters, including mobile phones, mobile base stations, Wi-Fi access points, television broadcasting, radio broadcast stations, and others. In addition to being free and green energy, scavenging this type of energy has advantages pertaining to the design of portable devices, which can be battery-free or at least have extended battery life, which can do without connectors and cables, and have freedom of mobility during charging and usage. On the other hand, wearable electronics have also attracted growing attention in recent years. Like other flexible electronics, wearable electronics are an appealing candidate for next-generation consumer electronics due to their light weight, ease and low cost of fabrication, and the abundance of inexpensive textile substrates. These advantages make them a good choice for designing radio frequency (RF) energy scavenging circuits like rectennas, hence the work on wearable rectennas or more generally the textile-based rectennas. These are not only suitable for powering or charging mobile devices, but they also have interesting applications in health-care monitoring, public safety, and body-centric and military communications.

The general block diagram of a rectenna, as illustrated by Jabbar *et al.* [6], includes a receiving antenna for collecting RF signals, a rectifying circuit, which converts the RF voltage to a DC voltage, and an impedance matching circuit in between. Rectennas are classified according to their sensitivity and their conversion efficiency. The sensitivity of a rectenna tells the range of the RF input power levels for which it can produce an output DC voltage. The conversion efficiency is defined as the ratio of the DC output power to the RF input power. Rectenna designs should focus on maximizing both the efficiency and the sensitivity, or on finding a suitable compromise between the two. In designing the antenna, many parameters of the received signal should be taken into consideration, like its frequency, intensity, polarization, and direction of arrival. The designed antenna could be narrow-band, multi-band, or wide-band, and should preferably be circularly polarized. In most cases, antennas used for energy harvesting are omni-directional, to well receive signals impinging from any azimuthal angle.

To design textile-based rectennas, the relative permittivity and tangent loss of the used textile material should be determined. This could be done by means of the parallel plate capacitor method illustrated by Zhang *et al.* [7], the reverse-engineering method used by Rishani *et al.* [8] and Haskou *et al.* [9], the automated fitting techniques presented by Declercq *et al.* [10], and the transmission/reflection line techniques given in [11–13]. Other methods are also possible depending on the design's goal frequency and bandwidth. The resonance method is based on measuring the resonant frequency peaks of a resonant cavity fixture when not loaded then when loaded with the material under study. On the other hand, the reverse-engineering method works by first designing an antenna assuming initial values for the permittivity and loss tangent of the textile, and then fabricating the

antenna and comparing its measured reflection coefficient results with those simulated with varied permittivity and loss tangent values. Comparing these results could be done manually or using automated fitting techniques. As for transmission/reflection line method, it is done by placing two microstrip lines of different lengths on the textile substrate and measuring their *S*-parameters to find their corresponding characteristics.

For wearable rectennas, the effect of the human body on the antenna performance is a concern. That is why a good antenna design with the smallest possible back lobes is necessary. In addition to implementing the antenna on a full ground plane, the more advanced technique of incorporating electromagnetic band gap (EBG) structures between the antenna's patch and the ground plane is also successful in decreasing the back lobes and hence limiting the effects of body proximity on the antenna characteristics, as illustrated by Rishani [14]. The use of EBGs in textile-based antennas can also offer major improvements in terms of radiation efficiency and impedance bandwidth.

In addition to an intensive review of the recent rectenna designs, this chapter deals with the electrical characterization of textiles and their use in the design of antennas and rectifier circuits for RF energy harvesting. Methods used to estimate the relative permittivity and loss tangent of textile substrates will be discussed through examples. The most recent wearable antenna designs will be reported, with focus on methods used to enhance their performance characteristics, and on their applications. The design and analysis of rectifying circuits used in RF energy scavenging will be examined, especially in terms of their sensitivity and conversion efficiency.

2 Electrical Characterization of Textiles for Antenna Design

One of the design challenges of wearable antennas is finding the characteristics of the textiles used as substrates. The relative permittivity (ε_r) and tangent loss $\tan(\delta)$ of such materials highly affect the behaviour and resonance frequency of the antenna and the design of the rectifying circuit. Several methods have been proposed and applied to find these parameters with varying precision, complexity, and cost.

2.1 Parallel plate capacitor

To find the relative permittivity of a substrate, a circular parallel plate capacitor was designed by Zhang *et al.* [7] as shown in Fig. 1, where the dielectric is sandwiched between the two parallel metallic plates. Such a configuration reduces the undesired fringing effect caused by corners of the square plates.

Originally, the input impedance is described using Green's function and is modified to match the proposed structure. The *0n*th modal impedance (Z_{0n}) of the structure can then be expressed, and a relation is established between ε_i, ε_r, and $\tan(\delta)$ with respect to Z^i_{0n} and Z^r_{0n}; Z^i_{0n} and Z^r_{0n} being the real and imaginary parts of Z_{0n},

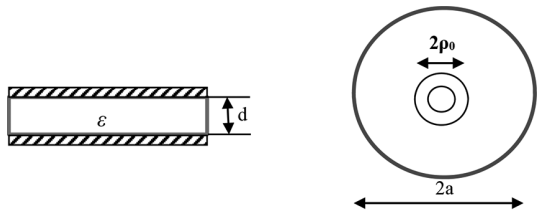

Figure 1: Geometry of the circular disk: (a) side view and (b) top view.

respectively. This approach is based on the measurement of the input impedance near a modal resonant frequency, at which the modal impedance Z_{0n} will dominate the input impedance. Consequently, at frequency very close to the resonant frequency, the complex permittivity can be obtained by replacing the modal impedance with the measured input impedance. At the 0*n*th modal resonant frequency, Z^i_{0n} is going to be zero and Z^r_{0n} is going to be maximum. Therefore, for higher mode case, the real part and imaginary part of the complex permittivity can be simplified as:

$$\varepsilon_r = \frac{k_{0n}^2}{\mu\omega^2}, \quad \varepsilon_i = \frac{H}{\mu\omega Z^r_{0n}} \tag{1}$$

The method proved to be accurate when the measurement frequency is close to the resonant frequency, but error increases as the measurement frequency shifts away.

2.2 Backward method

A simple reverse way was used by Rishani *et al.* [8] to determine the permittivity of Cordura [15] textile. An antenna, having stacked Cordura layers as a substrate, was simulated where an EBG layer was incorporated between the ground plane and the patch as in Fig. 2a. Simulations were based on an assumed ε_r = 1.9, at a resonant frequency of 1.575 GHz. Measurements of the fabricated prototype showed a shift of the resonant frequency to higher frequencies. The same design was simulated for various values of the permittivity until a matching frequency was obtained at ε_r = 1.5. The antenna was redesigned taking into account the new values of ε_r and results of the measured return loss, in Fig. 2b, matched those of simulation.

As illustrated by Haskou *et al.* [9], the relative permittivity and tangent loss of two textiles were determined by using quarter-wavelength stub-line band-stop filters whose substrate is either Jeans or Cordura. The filter was designed assuming a lossless Jeans substrate, having a relative permittivity of ε_r =1.5 at 800 MHz. The designed filter was fabricated as in Fig. 3 and the measurements of the return loss show a major shift in the frequency. The design was re-simulated for several values of ε_r and tan(δ) till the results matched the measurements at 800 MHz and 2.4 GHz. The same method was applied for Cordura fabric,and was verified by designing

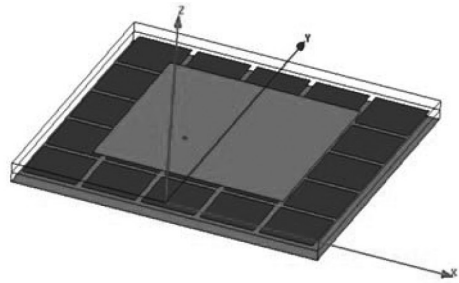

(a)

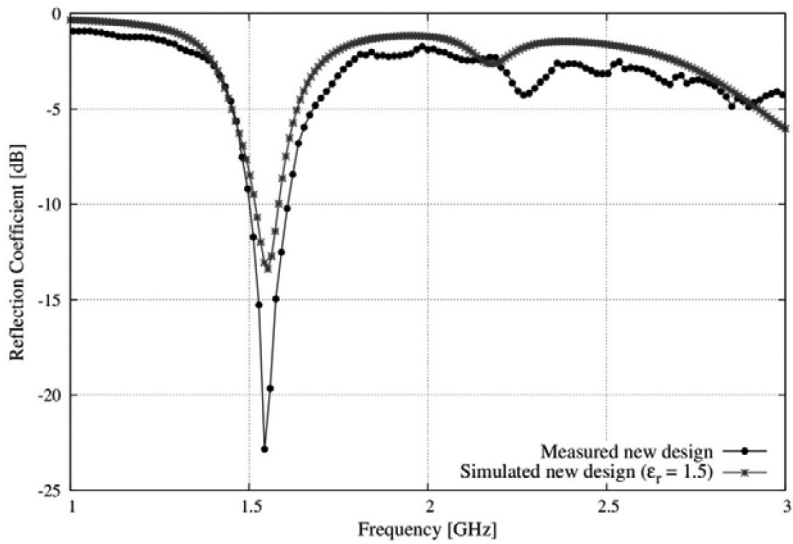

(b)

Figure 2: (a) Geometry of the proposed antenna showing patch, EBG layer, and ground plane. (b) Simulated and measured reflection coefficient of the redesigned antenna.

patch antennas on both Jeans and Cordura substrates, taking into consideration the found parameters. The designed antennas were fabricated and tested where measurements matched simulation results for both fabrics. The fabricated patch antennas are shown in Fig. 4, along with the results of the Jeans-based design.

2.3 Automated fitting techniques

Another technique of comparing and fitting simulated with measured results to find permittivity and loss tangent of a textile was applied by Declercq *et al.* [10]. The fitting technique is automated optimization based on kriging surrogate

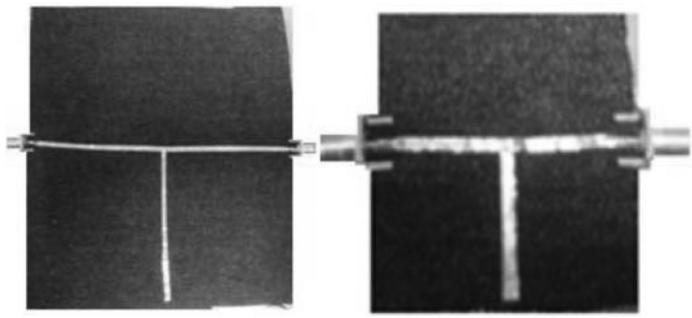

(a) (b)

Figure 3: Prototypes of the fabricated Jeans-based band-stop filters at (a) 0.83 GHz and (b) 2.34 GHz.

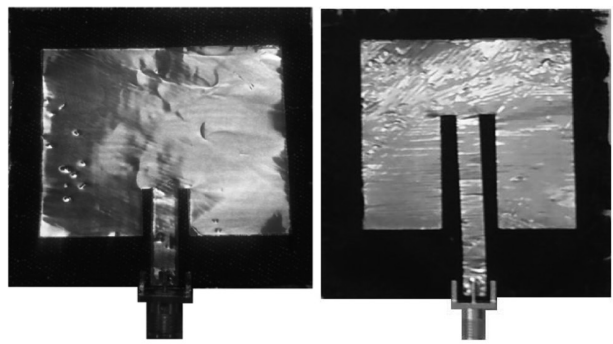

(a) (b)

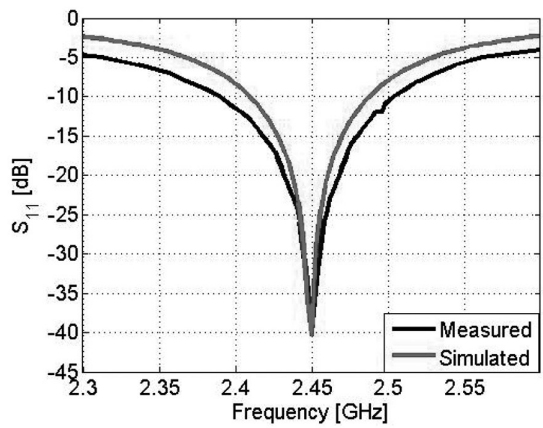

(c)

Figure 4: Prototypes of the (a) Jeans-based and (b) Cordura-based fabricated patch antennas and (c) simulated and measured S_{11} of Jeans-based antenna.

models. Initial values of the permittivity and tangent loss were assumed to design an antenna resonating at 2.45 GHz and measure its reflection coefficient $|S_{11}|$. The mean squared error (MSE) is used to minimize the error function between the measured and simulated $|S_{11}|$, where the cost function is first created by an initial set of 24 points generated by an optimal maximum Latin hypercube design. Then using the DIRECT algorithm, the improvement function was optimized to determine the next sample to evaluate. Seventy-one samples were evaluated and the optimal electromagnetic properties yielding a minimal MSE were found and are displayed in Fig. 5. The same method was applied to two different antennas, one having a four-layer plain woven aramid fabric substrate of thickness 1.67 mm, and the other having nonwoven polypropylene fabric of thickness 3.6-mm copper foil, and the substrates were glued using an adhesive sheet.

Textile characterization using the surrogate method was also applied by Declercq *et al.* [16] taking into consideration the relative humidity levels and the sensitivity of each material to humidity. The effective conductivity of electro textiles was also studied.

2.4 Coaxial resonator method

Nagy and Szalay [17] presented a coaxial resonator measuring system to determine the dielectric parameter of materials. The technique is based on designing a coaxial resonator, measuring the scalar scattering parameter $|S_{21}|$ when not loaded, and finding the complex dielectric constant using the quality factor. Two coaxial resonators with different inner conductor diameters were designed and used, to determine both the real and imaginary parts of ε_r. The RF measurements, frequency sweep over the range 650–850 MHz, and signal strength were measured using two ISM band RF transceivers controlled by PC using microcontroller, placed on a double-sided PCB substrate with full ground.

The resonant frequency found from the peak detection of S_{21} curve was used to estimate $Re\{\varepsilon_r\}$. The estimated $Re\{\varepsilon_r\}$ and the Q factor determined from the peak from 3 dB bandwidth of the resonator S_{21} determine the value of $Im\{\varepsilon_r\}$. Measurements of cross talk between these two tranceiving circuits were also investigated.

A similar technique was implemented by Szalay *et al.* [18] and used for several textile types. A frequency sweep range of between 480 and 900 MHz is considered. The input and output loop positions, sizes and the coaxial inner and outer conductor diameter, and resonator length have been optimized to maximal sensitivity in the range $Re\{\varepsilon_r\} = 2,...,15$ and $Im\{\varepsilon_r\} = 0.1,...,0.7$. The finite element method was used to model the resonator, using measurements of known parameter materials and changing the geometry parameters of the model accordingly. The second step was to generate a database containing resonance curves in function of material parameters. The electrical parameters are then determined using curve-fitting techniques in Matlab. Results show the high resolution of this measuring technique of the complex dielectric constant.

Kehn *et al.* [19] provided theoretical formulation of a permittivity measurement technique using a coaxial transmission line structure with dielectric annular rings using a quadratic curve-fitting approach. The mode-matching technique and the

method of moments with cavity/waveguide Green's functions were used to treat the connected series of coaxial sections. In another publication, Kehn *et al.* [20] presented numerical results of a typical coaxial fixture relevant to the measurement technique presented in their earlier publication.

2.5 Transmission line method

The transmission line method is another common technique used to find the permittivity and tangent loss of a substrate as in [11–13]. Declercq *et al.* [21] used the same method combined with the matrix-pencil technique to reduce the perturbations in the transmission parameters of the deembedded transmission line. The two transmission lines of length l_2 and l_1, with $l_2 > l_1$ are characterized by their complex propagation factor $\gamma = a + j\beta$ and the unknown characteristic impedance Z_0. Deembeding is achieved by measuring the *S*-parameters of the two microstrip lines, and using the measurements to build their corresponding scattering transfer cascade matrix defined by Lee and Nam [11]. These matrices are then expressed in terms of the coax-to-microstrip discontinuities and to the lossy transmission line with length $\Delta l = l_2\text{-}l_1$. Using eigenvalue equations, the propagation factor can be determined, and then once β is known, $\varepsilon_{r,eff}$ follows from $(\beta/k_0)^2$, and the dielectric constant is calculated using the transmission line calculator Linecalc from Agilent's Advanced Design System.

Assuming the conductive layer is lossless, the tangent loss of the substrate can be calculated as

$$\tan(\delta) \approx 0.0366 \frac{a_d \lambda_0 \sqrt{\varepsilon_{r,eff}}(\varepsilon_r - 1)}{\varepsilon_r(\varepsilon_{r,eff} - 1)}$$

The use of the matrix-pencil method allows minimizing the effect of the geometrical inaccuracies of the transmission line structures, non-identical coax-CPW transitions, and parasitic mode excitation, which are interpreted as an unknown noise distribution to adjust the eigenvalue equation of the propagation factor. The matrix-pencil method then performs optimal fitting of a series of complex exponentials on noise contaminated data.

Verification of the proposed method was done by applying it to an antenna whose substrate is RT/Duroid 5870 of known permittivity. The method was then tested on three different fabrics with a very good match between measured and simulated values of S_{11}. The permittivity was also noted to change when the conductive material is an electro textile rather than a conductor.

3 Textile Antennas and Applications

Wearable antennas have potential applications in diverse areas including personal entertainment, wearable computing, soldier communications, security systems, remote identification, personnel tracking, health monitoring, navigation aid,

rescue operations, and RF energy harvesting as illustrated by Nepa and Manara [22] and Monti *et al.* [23]. The increasing importance of body-centric communications within the sphere of personal area networks (PANs) and body area networks (BANs) has also led to increasing demand on wearable antennas as outlined by Rais *et al.* [24].

The differing designs and shapes of wearable antennas, more generally of the textile-based antennas, reflect their diverse fields of usage. Some characteristics are common to all designs, while others vary with the application, from the material type, to the form of radiating part, to the feed, etc.

3.1 Medical applications

Medical applications are among the most promising applications of textile-based antennas due to the wide demand on telemedicine and wireless health monitoring systems. Textile-based antennas, embedded in the clothing of the patients or in their bed sheets and their blankets, can be used to monitor their heart rate, body temperature, and other vital signals.

A fully-textile-based washable ultra-wideband (UWB) antenna for medical monitoring applications is reported by Osman *et al.* [25]. Herein, the substrate is made of the flannel fabric, which is a 100% cotton material. Its relative permittivity is $\varepsilon_r = 1.7$. The patch and the partial ground plane are based on conducting threads made of silver-plated nylon, which ensure strength and conductivity in addition to washability and resistance to environmental conditions. The antenna is 6×6 cm^2, where the substrate is 3-mm thick. It has a 17-GHz impedance bandwidth.

Khaleel *et al.* [26] proposed a printed Yagi antenna for applications in telemedicine and wireless body area network (WBAN). A metal button is used, due to its low profile, rigidness, robustness, and easy feed, in addition to its low cost and ease of integration into pieces of cloths. The antenna has a perfect electric conductor (PEC) ground and microstrip Yagi, formed of driven element, directors, and couplers. The two PEC layers are separated by a thick substrate with a high permittivity ($\varepsilon_r = 6.6$). The design, which is an enhancement over other button antennas using ordinary rectangular or circular patches, shows very good matching at 2.45 GHz (frequency used for WBANs) and has a semi-directional pattern to avoid unnecessary radiation towards the body and a gain of 6.7 dB.

Another medical application of textile-based antennas is in the remote measuring of heart rate. Fletcher and Kulkarni [27] propose the use of a Doppler radar system embedded in a piece of cloth or a blanket. The system that measures heart beats by sending and receiving microwave beams consists of an oscillator, an antenna, a single mixer, and a baseband band-pass filter. The antenna is a microstrip rectangular patch fabricated on FR-4 epoxy ($\varepsilon_r = 4.2$), and having a return loss of 18 dBm and 4 dBi directional gain.

In a similar work presented by Reina-Tosina *et al.* [28], a wearable sensor to monitor patient movements is designed and constitutes of an intelligent accelerometer unit connected to a personal server via a PAN. The communication link

is based on Zigbee, due to its low power consumption and ability to support larger number of nodes compared with Bluetooth. A rectangular patch is used and is fed by aperture coupling. Such an implementation allows having the circuit components on the bottom substrate, thus making efficient use of the antenna size.

Another method of monitoring heart rate with wearable sensors is by Mandal *et al.'s method* [29], where heart beats are heard via microphones. The system's circuit has a PLA (Programmable Logic Array) chip that when necessary sends an alarm signal through the antenna to the base station. The signal transmitted is modulated by backscatter modulation technique that allows bulky signal processing to be done at the level of the base station thus reducing the circuit's complexity and power consumption. The antenna implemented is a circularly polarized loop antenna that is less sensitive to propagation barriers. Using a 2.4-GHz frequency allowed having a small-sized antenna. The whole tag was placed on 1-cm thick dielectric foam, to reduce radiations towards the body, and reduce the effects of the body tissues on the system's performance. The chip also has the capability of harvesting radiated RF power, making it possible to have a battery-free tag.

Sensors and body sensor networks (BSN) in particular and their usage in telemedicine were discussed by Wang *et al.* [30]. BSN nodes of low-power consumption and small size are distributed on the body to collect physiological data and they communicate with an off-body base station in the same network via antennas. Each of these nodes is made up of a BSN node board, antenna board, and a battery board with a charger IC. The antenna FR4 board has a microstrip square-shaped loop antenna, operating at 915 MHz. Loop antennas, acting as magnetic dipoles, are less affected by dielectric changes and thus are less sensitive to body tissues than dipoles or patches.

In designing BSNs, array antennas are used due to the high data rates they provide, yet mutual coupling (MC) is a disadvantage. Zhang and Ser [31] analysed the effect of MC on antenna behaviour and their effects on BSNs used in medicine. The resulting equations and simulations ascertain the well-known property that MC increases as the distance between array elements decreases. This increase in MC decreases the efficiency of the antenna and the data rates as well.

Low-power wearable antennas have several other usages in medical domain, like using them for the electroencephalogram braincap. This technique, proposed by Carmo *et al.* [32], allows monitoring the brain activity while the patient has the ability to move around instead of being bound to many wires. The technique is based on using the same brain cap but replacing the wired electrodes with electrodes having an RF transceiver to communicate with monitoring instrumentation used by doctors. The UMC RF 0.18 μm CMOS process was used to maintain low-power consumption, small size, and small voltage supply. At the antenna level, digitally controlled switch circuitry is used to switch between transmission and reception modes. A commercial gigaAnt loop antenna was used having a bandwidth of 401 MHz and 55% efficiency in the frequency range 2.4–2.5 GHz.

3.2 Safety and military applications

Textile-based antennas are also very suitable for safety and military applications. On modern battle fields, soldiers are to be connected to each other and to a command center to enhance the situation awareness as illustrated by Lilja and Salonen [33]. In such scenarios, wearable antennas are an optimal solution especially that military cloths are usually made up of thick fabric and antennas can be easily integrated within their layers. Textile-based antennas can as well be embedded into protective clothing of rescuers and firefighters.

Vallozzi *et al.* [34] presented an antenna design that can be used for rescue applications. This design takes into consideration the fact that rescuers work in harsh environments and the antenna must overcome channel fading and be robust. For that, a dual polarized textile patch antenna is used with a coaxial line feed. The design that works in the ISM band (2.4–2.4835 GHz) allows for polarization diversity. The patch and ground are made up of electrotextiles ShieldIt and Flectron, respectively, and are separated by a protective foam substrate that is already used in the protective garments of the rescuers. The antenna has a 6-dBi gain along the broadside direction with perfect isolation between the ports. The antenna can transmit and receive at the same time, and the presence of the human body in its vicinity leaves little effect on its performance.

An antenna design for integration into firefighters' garments is described by another publication of Vallozzi *et al.* [35]. The patch and ground layers are made up of the ShieldIt and Flectron electrotextiles, respectively, whereas the substrate is a protective, shock absorbing, fire retardant, and water repellent foam used in firefighters' suits. Such materials permit the antenna to keep its characteristics for very harsh environments. The antenna is based on a rectangular patch with a wide slot. Similar to this work, this design has two feeding points implemented to insure that two signals with different polarization can be simultaneously excited, also allowing for transmission and reception at the same time. On the other hand, two antennas are placed on a single firefighter's suit, one in the back and the other in the front. Such a topology, allows for fourth-order diversity by having two antennas each with second-order diversity, which leads to a significant improvement in terms of the bit-error rate. The characteristics of the antennas are also studied for both ports off-body, on-body, and with the firefighter holding his usual oxygen bottle on his back. The presence of the bottle affects the gain a little at both ports, but the performance is still good.

One type of antenna in use for military applications is integrated into the soldier's helmet. The antenna studied by Tillery *et al.* [36] is an adaptive cylindrical four-element array; each element is a spiral-mode microstrip, mounted on the helmet. The system has 15 different radiation patterns, and the control circuit uses threshold switching among them. This CMOS circuit has very low-power consumption. It requires 3 V power supply mounted inside the helmet and consumes about 4 mW to switch from one pattern to another.

A flexible wearable E-shaped patch antenna that can be placed on a soldier's arm is presented by Cibin *et al.* [37]. The antenna had an omni-directional pattern.

The patch is made up of thin copper layer, and the ground is based on a conductive non-woven fabric. They are separated by a thick foam used in orthopaedics that does not absorb moisture. Although the antenna performance is affected by different curvatures of bending around the arm, it still demonstrates good matching over the band 360–460MHz, with an enhanced gain over the body-worn dipole.

3.3 WLAN applications

The widest application of textile-based antennas would be in the prevailing wireless local area networks (WLANs). Sanz-Izquierdo *et al.* [38] proposed a button antenna characterized by its robustness, high camouflage, and ease of integration into cloths. The conducting part is the metallic button itself, made up of a button-shaped structure and a metal disk connected to the ground. Additional shorting pins are added to enhance the bandwidth while keeping a small size. This antenna has an omni-directional pattern, is able to communicate with other systems that might be attached to the body, and has a gain of 1–3.5 dB within the 2.4 and 5.2–5.5 GHz WLAN bands.

Sanz-Izquierdo and Batchelor [39] presented a simple antenna design optimized to be operable at 2.4 and 5 GHz WLAN bands is the metallic belt buckle. The buckle's structure is the antenna, connected to an SMA via a microstrip line, with an optimal ground plane, all separated by a denim substrate ($\varepsilon_r = 1.4$). This belt antenna has a gain of 2.8 and 4.5 dBi at 2.45 and 5.25 GHz, respectively, and a radiation pattern very similar to a planar monopole on a small ground plane.

Flexible planar inverted F-antennas (PIFAs) are used by Salonen *et al.* [40] for Bluetooth applications. The wired flexible PIFA, which is to be placed on the human arm, has a flexible substrate with $\varepsilon_r = 3.29$. To overcome the small bandwidth disadvantage, the authors propose adding an arm to the PIFA, operating at 2.45 GHz.

The design proposed by Yilmaz *et al*. [41] for 2.4 GHz WLAN is an antenna whose patch and ground plane are made of low conductivity polymer inks or carbon nano-structured inks, and separated by a substrate whose dielectric constant is $\varepsilon_r = 2.2$. For comparison, the same design was fabricated using a copper conductor, and the results show that using a material with low conductivity degrades the reflection coefficient and the gain, but the performance remains acceptable with materials having conductivity values higher than 10^4 S/m (copper's conductivity is 5.7×10^7 S/m).

3.4 Millimetre wave communications

Textile antennas can also be used for communications at millimetre waves. A textile Yagi-Uda antenna for on-body communications has been proposed by Chahat *et al.* [42]. It is based on a 0.2-mm thick fabric extracted from a cotton shirt. The dielectric properties found for the employed textile are the following: $\varepsilon_r = 1.5$ and $\tan(\delta) = 0.016$. A flexible copper foil with thickness of 0.07 mm is used for all conductive elements. The antenna operates in the 57–64 GHz band. Assessment results in free space and on a skin-equivalent phantom show that the reflection

coefficient is very slightly affected by the human proximity, but the antenna gain and efficiency strongly depend on the separation between the antenna and the phantom.

Another antenna array for off-body communications in the 57–64 GHz band has been reported by Chahat *et al.* [43]. The 0.2-mm thick textile substrate, which is based on a cotton woven fabric, has been characterized in the V-band using the open stub technique, and the dielectric properties are found to be $\varepsilon_r = 2$ and $\tan(\delta) = 0.02$. Flexible 0.07-mm thick copper foils are used for the conducting parts. Measurements are done in free space and on a skin-equivalent phantom. A comparison of the results shows that the human body has little impact on the antenna performance. The authors have also numerically and experimentally investigated the influence of bending under severe conditions. They report that bending has a small impact on the reflection coefficient and antenna gain.

3.5 Textile antenna design improvements

Different methods are used to achieve robust transmission and reception capabilities with textile antennas. These include the optimized positioning of the antenna on the body, for wearable antennas, the use of multiple antennas well distributed on the body, the design of circularly-polarized textile antennas, and the use of EBG structures.

A wearable textile multi-antenna system suitable for integration into a jacket has been proposed by Castel *et al.* [44]. The authors derive the optimal distribution and the minimum number of on-body antennas required to ensure signal levels large enough for an in-body medical application, in this case an endoscopy capsule.

Circular polarization is more robust as opposed to linear polarization because it guarantees signal reception independently of antenna orientation. It is usually achieved by cutting special slots or notches in the patch or ground plane, or by feeding the patch with a 90° phase shift. A wideband wearable circularly polarized antenna for low-power transmission in the 2.45 GHz ISM band is presented by Lui *et al.* [45]. The antenna consists of two layers, where the top one is the conductive fabric and the bottom layer is the felt substrate. A Flectron self-adhesive EMI shielding sheet is used for the conductive part, due to its flexibility and high conductivity. A 1-mm thick acrylic self-adhesive felt is chosen for the substrate. Its dielectric constant and loss tangent are determined as 1.5 and 0.02, respectively. A coplanar waveguide (CPW) feed is used. The L-shape of the feed line produces the necessary x and y components of magnetic current for circular polarization. Results show that this antenna has a 44% 10 dB impedance bandwidth and a 23% 3 dB axial ratio bandwidth on a human body. A circularly polarized wearable antenna for RF energy harvesting in the 2.4 GHz band is reported by Haskou [46] where the circular polarization is obtained by cutting an L-shaped slot at one corner of a rectangular copper-foil patch placed over a Jeans-based substrate. A photo of a fabricated prototype of this antenna is shown in Fig. 5.

The use of EBG structures offers the advantages of reducing the backward radiation towards the body of wearable transmitting antennas, and also limiting the

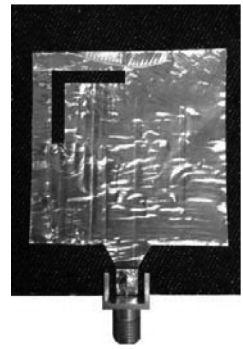

Figure 5: A circularly polarized Jeans-based wearable antenna for the 2.4 GHz band.

effect of proximity to the body. A dual-band wearable antenna on an EBG substrate is presented by Zhu and Langley [47]. A design that combines circular polarization and the use of EBGs is presented by Rishani [14]. A coax-fed rectangular patch is used and is separated from an EBG-layer made from square conducting patches by a Cordura fabric layer. A second Cordura fabric layer separates the EBG from a full ground plane. A flexible copper foil is used for all conductive parts. Circular polarization is achieved by cutting two joined rectangular slots in the middle of the patch. The geometry of this antenna, the axial ratio, the reflection coefficient, and the polar two-dimensional power pattern at $\Phi = 0$ are shown in Fig. 6a–d, respectively.

This antenna is made for GPS applications. The inclusion of the EBG layer reduces the backward scattered radiation and limits the effect of body proximity on the antenna performance. This antenna can be used in a multi-antenna configuration where the position of each element is optimized to get the best space diversity, or in a configuration with both RHCP and LHCP versions to benefit from polarization diversity.

In the flexible antenna design presented by Khaleel *et al.* [48], an artificial magnetic conductor (AMC) ground plane is used to isolate the user's body from undesired electromagnetic radiation, in addition to minimizing the antenna's impedance mismatch caused by the proximity to human tissues. The design, which is intended for telemedicine and WBAN applications in the 2.45 GHz ISM band, is based on an M-shaped CPW-fed monopole printed on a 50.8-mm-thin kapton polyimide substrate with a dielectric constant of 3.5 and a loss tangent of 0.002. The AMC ground itself is made of 3′3 slotted Jerusalem Cross unit cells designed to resonate at the same operating frequency of the antenna, and is printed on a flexible vinyl substrate with a 1.5-mm thickness and a dielectric constant of 2.5. The total size of the AMC structure is 65.7 mm × 65.7 mm. Results show a reduction of 64% in the specific absorption rate values compared with the same antenna without the integration of AMC, and a low susceptibility to performance degradation in terms of return loss and shift in the resonant frequency when conformed on curved surfaces.

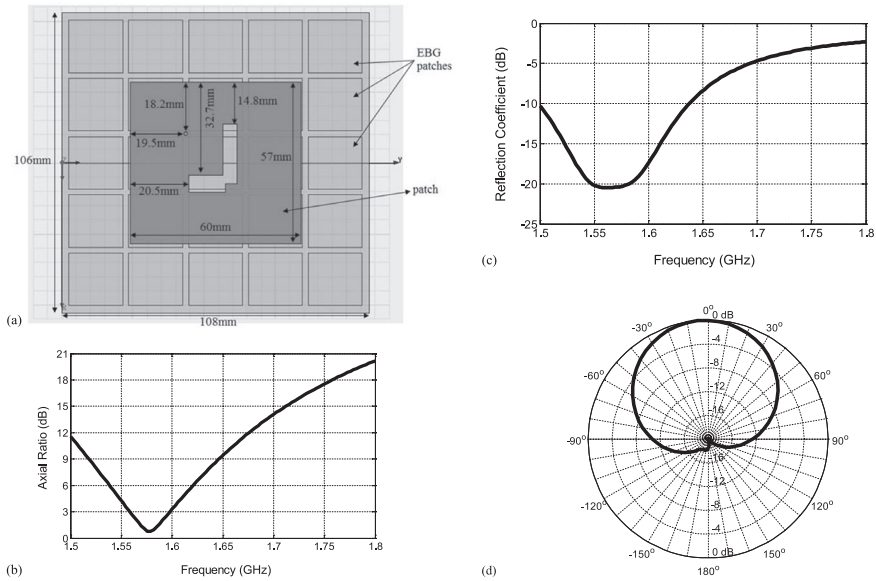

Figure 6: (a) A circularly polarized wearable antenna over an EBG substrate for GPS applications, (b) axial ratio, (c) reflection coefficient (S11). (d) Polar two-dimensional power pattern at $\Phi = 0$.

4 Rectifying Circuits

An important component in designing a rectenna is its high performance characterized by a high RF-DC conversion efficiency. This efficiency, defined by Olgun *et al.* [3], as the ratio between the output DC power and the incident RF power:

$$\eta = \frac{P_{DC}}{P_{RF}} = \frac{V_{DC}^2}{R_L P_{RF}} \tag{2}$$

where η is the rectenna conversion efficiency, P_{DC} is the rectenna output DC power, P_{RF} is the RF incident power, V_{DC} is the output DC voltage, and R_L is the load resistance.

Since a rectenna system is usually composed of an antenna, an impedance matching circuit, and a rectifying circuit, the total efficiency of the rectenna is the product of the efficiency of the three components as illustrated by Kim [4]

$$\eta = \eta_{antenna} \cdot \eta_{match} \cdot \eta_{rectification} \tag{4}$$

In (4), $\eta_{antenna}$, η_{match}, and $\eta_{rectification}$ are the efficiency of the antenna, the impedance matching circuit, and the rectifying circuit, respectively. The rectifying circuit

efficiency is mostly dominated by the diode's efficiency where most of the losses in the circuit come from the diodes electrical parameters as illustrated by Merabet *et al.* [5]. The selection of the rectifying diodes depends on the targeted frequency band and the expected input power. The diodes' series resistance, parallel resistance, junction capacitance, junction voltage, and operation frequency band are all factors to be taken into consideration. A zero-bias diode is more convenient to be used in small signal applications. A diode with small junction capacitance and parallel resistance will be less sensitive to the frequency variation and hence can be used in wide band applications. A big series resistance will lead to high losses and hence will drop the conversion efficiency. Olgun *et al.* [3] chose Agilent HSMS-2852 diodes because their performance is optimized in the targeted frequency band; they do not require any external biasing and they have a high saturation current. However, the main drawback of the selected diode is that it has a high series resistance causing higher resistive losses.

In the literature, all the different rectifying circuits were used. Marian *et al.* [49] tested half wave series- and shunt-mounted diode rectifying circuit and compared with a single-stage voltage doubler. Figure 7 shows half wave series-mounted diode rectifier. The circuit works as follows: When the input voltage is superior to the diode's junction voltage ($V_{in} \geq V_D$), the diode D_1 will be on and the capacitor will start charging. When ($V_{in} < V_D$), the diode D_1 will be off and the capacitor will discharge through the load. The amplitude of the ripples will depend on both the load and the smoothing capacitor.

Figure 8 shows a shunt-mounted diode half wave rectifier. The circuit works as follows, when the input voltage is less than the negative of diode's junction voltage ($V_{in} < V_D$), the diode D_1 will be on and the capacitor C_1 will start charging. When ($V_{in} \geq V_D$), the diode D_1 will be off and voltage of $2V_{peak}$ will be divided between the inductor L_1 and the load $Z_L = R_L//C_2$.

A half-wave rectifier requires a minimum voltage of V_D to function and hence can be used in low-power scenarios. Moreover, a half-wave rectifier has only one capacitor and hence can provide relatively larger bandwidth compared with other circuits. Half-wave rectifiers' simplicity makes them convenient to be directly integrated in the antenna structure. However, the main drawback of a half-wave rectifier is its low efficiency.

As illustrated by Hagerty *et al.* [50], two rectenna arrays, shown in Fig. 9, where the rectifying diodes were directly integrated in the antenna structure, are designed.

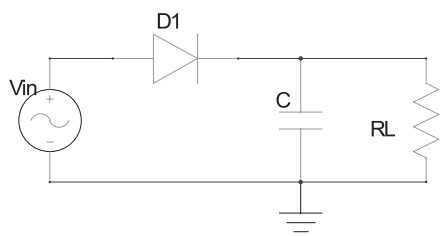

Figure 7: Schematic of a series-mounted diode half wave rectifier.

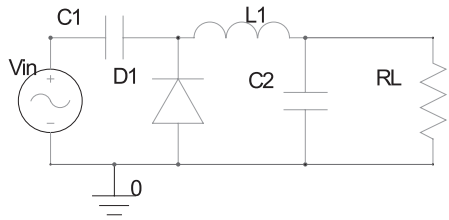

Figure 8: Schematic of a parallel-mounted diode half-wave rectifier.

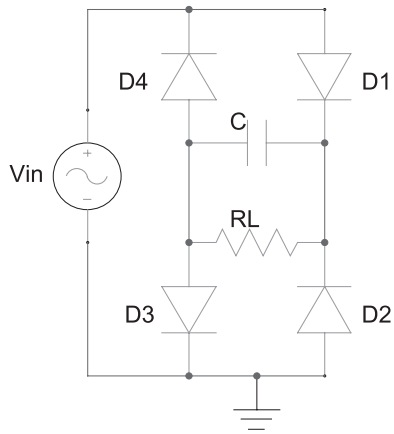

Figure 9: Schematic of a bridge full-wave rectifier.

The first rectenna is a grid array that achieves wide bandwidth functionality (4.5–8 GHz) and dual linear polarization. The second rectenna is a spiral array with both left- and right-hand circular polarization and a wide band (8.5–15 GHz). However, asmentioned above, half-wave rectifiers have relatively low efficiencies. Hence, maximum measured efficiencies of 35% and 45% are reported.

Kim [4] used a full-wave bridge rectifier and measured efficiencies up to 45% were reported. Figure 18 shows a full-wave bridge rectifier schematic. The circuit functions as follows; when the input voltage is greater than double the diode's junction voltage ($V_{in} > 2V_D$), the diodes D_1 and D_3 will be on and the other two diodes will be off; hence, the current will flow through the branch D_1 and load D_3. When ($V_{in} < 2V_D$), the diodes D_2 and D_4 will be on and the other two diodes will be off and the current will flow through the branch D_2 and load D_4. It can be noticed that the current direction is the same in both phases and hence the negative phase is rectified. It can also be noticed that a bridge rectifier requires a minimum voltage of ($2V_D$) to function so it is more convenient for high signal applications.

Taris *et al.* [51] used a Greinacher (Cockcroft-Walton) voltage doubler rectifier, and at input levels as low as P_{in} = 10 dBm, a measured output voltage of V_{DC} =1.1 V was reported. Figure 10 shows a Greinacher voltage doubler schematic. The

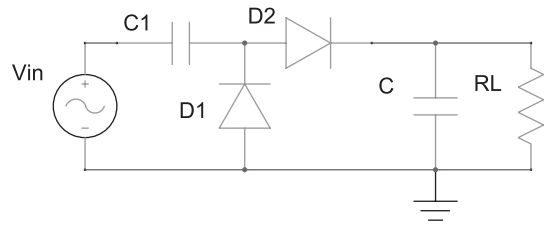

Figure 10: Schematic of Greinacher voltage doubler rectifier.

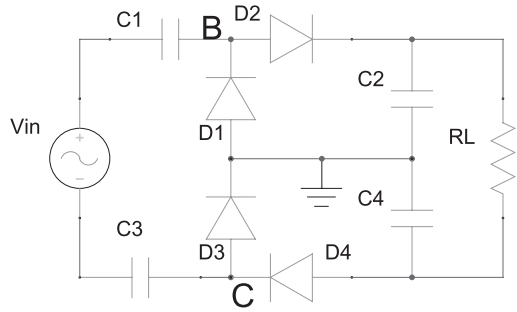

Figure 11: Schematic of modified Greinacher voltage doubler rectifier.

functionality of the circuit is as follows: when the input voltage is ($V_{in} < V_D$), the diode D_1 will be on and D_2 will be off and the capacitor C_1 will charge to a maximum voltage of (V_{in}–V_D). When ($V_{in} > V_D$) the diode D_2 will be on and D_1 will be off; hence, an input voltage of $2(V_{in}–V_D)$ (from both the input voltage and the capacitor's one) will appear on the load. It can be noticed that the output DC voltage is approximately double the peak voltage of the input voltage; hence, this circuit can be used in applications that require high-voltage levels.

A modified Greinacher voltage doubler rectifier was proposed by Olgun *et al.* [52]. A schematic of the proposed circuit is shown in Fig. 11.

The proposed circuit operates as follows: C1 and D1 shift the input voltage up at node B to be rectified by D2 to appear across the load. C3 and D3 shift the voltage down at node C to be rectified by D4 and C4 to appear across the load. After reaching equilibrium, the circuit provides a constant output current and voltage to the load.

Muramatsu and Koizumi [53] used a six-stage Dickson charge-pump voltage doubler and a measured DC output voltage as high as $V_{DC} \approx 3.7V_{peak}$ was reported, where V_{peak} is the peak voltage of the incident RF signal. A schematic of an n-stage Dickson charge-pump voltage doubler is shown in Fig. 12. Dickson charge-pump voltage doubler voltage is given by

$$V_{load} = 2n(V_{peak} - V_D) \tag{5}$$

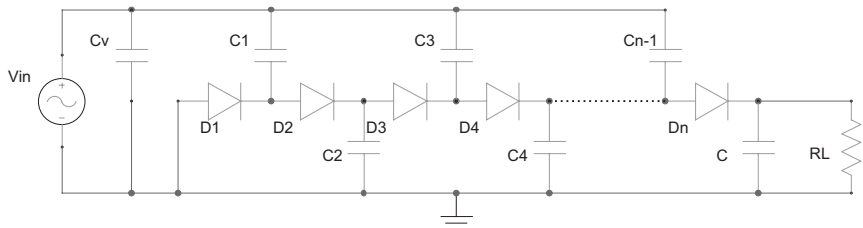

Figure 12: Schematic of *n*-stage Dickson voltage doubler rectifier.

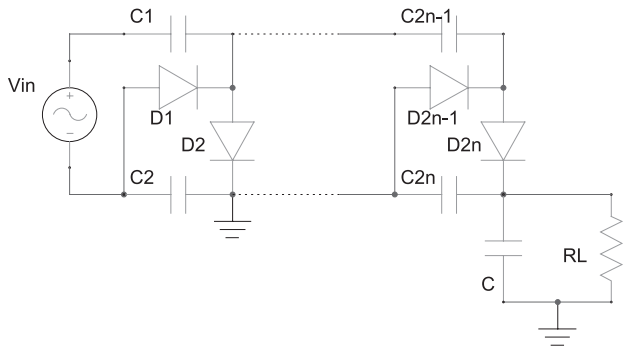

Figure 13: Schematic of *n*-stage Villard voltage doubler rectifier.

The main drawback of this circuit is the voltage drop due to the diode junction voltage, which is *n*-times the drop caused by one diode. One other problem with this circuit is the transient period before the output voltage reaches its maximum value. In this publication, for RF frequency of 954 KHz, a transient period of about 1 h was reported before the output voltage reached its maximum.

A four-stage Villard voltage doubler rectifier was also reported by Devi *et al.* [54]. Therein, for input levels as low as $P_{in} = 0$ dBm a measured DC output voltage of $V_{DC} \approx 2.3$ V was reported. A schematic of an *n*-stage Villard voltage doubler is given in Fig. 13.

The DC output voltage of a Villard circuit is given by

$$V_{DC} = \frac{nV_o}{nR_o + R_L} \tag{6}$$

where V_o is the open circuit output voltage of a single stage and R_o is the internal resistance of the single stage. Schottky diodes have good characteristics compared with junction diodes. However, they are not available in CMOS technology.

Arrawatia *et al.* [55] open the door of new trends in the design of rectifying circuits, which is using CMOS technology. Accordingly, Karolak *et al.* [56]

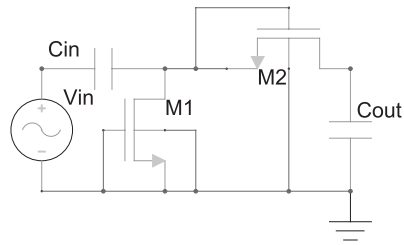

Figure 14: Schematic of traditional CMOS-based voltage doubler rectifier

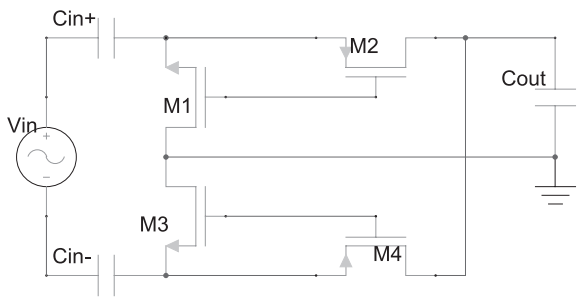

Figure 15: Schematic of cross-coupled voltage doubler rectifier.

designed a modified cross-coupled CMOS-based voltage doubler circuit and compared with traditional CMOS-based voltage doubler. Figure 14 shows a traditional CMOS-based voltage doubler.

Schematic of the modified differential cross-coupled voltage doubler, as reported by Karolak *et al.* [56], is shown in Fig. 15. An *n*-stage circuit will achieve an output voltage of

$$V_{\text{load}} = 2n(V_{\text{peak}} - V_{\text{f}}) \tag{7}$$

Jabbar *et al.* [6] designed a modified CMOS-based Villard voltage doubler circuit and compared with traditional CMOS-based Villard voltage doubler. The proposed design therein, for an input power of 0 dBm, achieves 160% increase in the simulated output power compared with the traditional circuit. Figure 16 shows the schematic of the modified Villard voltage doubler.

In a very recent work done by Hao *et al.* [57], a 71 GHz RF energy harvesting based on CMOS technology was integrated in a temperature sensor. To increase the efficiency of the circuit, the authors used modified inductor-peaked diode stage. The resonance of the inductors and the capacitors C_{gs} will make the voltage swing at the gate higher than at the drain and hence will make the diode forward resistor lower. Figure 17 shows the circuit proposed in this publication.

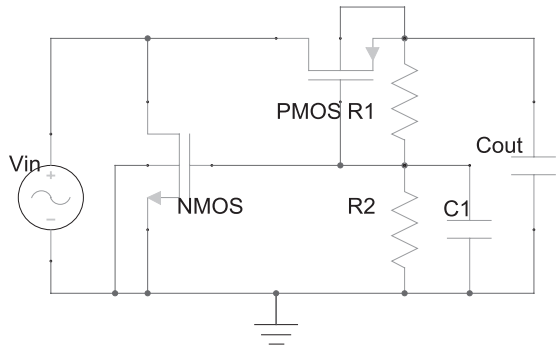

Figure 16: Schematic of the modified Villard voltage doubler rectifier.

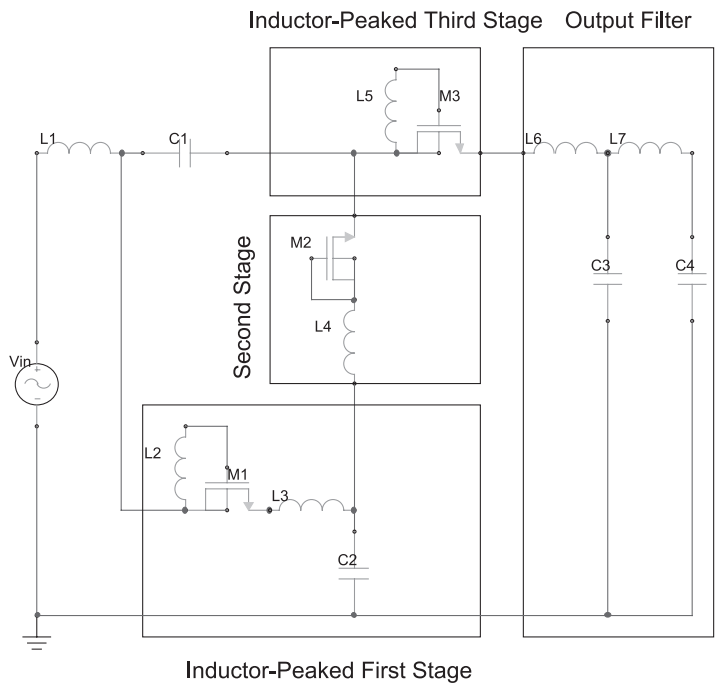

Figure 17: Schematic of the three-stage inductor-peaked rectifier.

Huyen *et al.* [58] designed a five-stage full-wave differential rectifier based on CMOS technology, which was adapted. For input levels as low as 15 dBm the circuit introduced DC voltages of 1.7 V. Figure 18 shows the circuit proposed in this work.

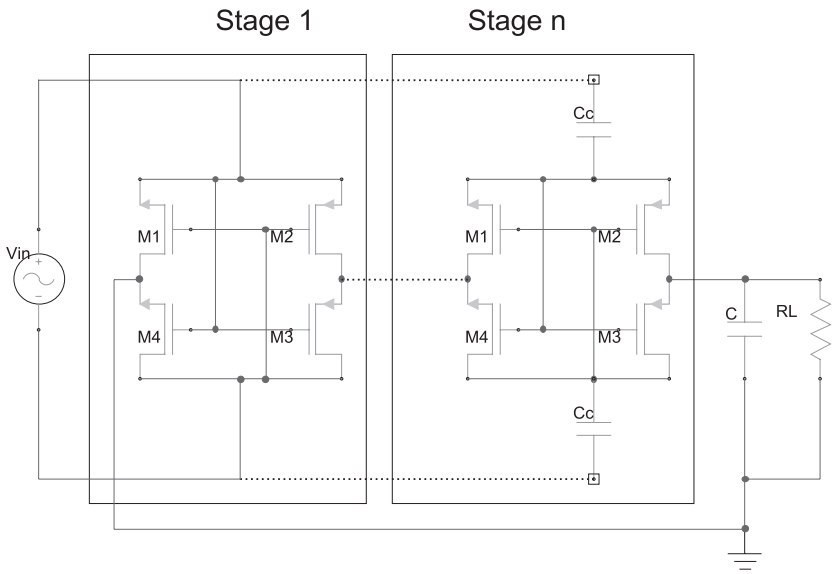

Figure 18: Schematic of the *n*-stage full-wave differential rectifier.

5 Review of Recent Rectenna Designs

In the last few years, as portable electronic devices have become a part of human life, interest in building rectennas to power these devices becomes a necessity. These rectennas operate at known wireless transmitting frequencies that range from UHF to microwave.

Monti *et al.* [23] designed and fabricated a UHF textile rectenna consisting of a compact patch antenna using a conductive nonwoven textile on a bi-layer substrate of Pile and Jeans. The circuit used to rectify the RF signal received by the antenna is a full-wave bridge rectifier on a layer of Jeans attached to the ground plane of the antenna. It was fabricated by using RF Schottky diodes, and the same conductive fabric was used for the patch antenna. From measurements, with respect to a 50 Ω impedance, the textile patch antenna exhibits a relative impedance bandwidth of 2.8% centred at 892 MHz. As for the rectenna, experimental data demonstrate that the proposed device has a maximum conversion efficiency of about 50% at 876 MHz.

A square patch antenna based on a 1.3-mm thick Jeans substrate, shown in Fig. 14, was designed by Haskou [46] to operate at 2.45 GHz. A transitional impedance matching was added to set the input impedance of the designed antenna to 50 Ω at the desired frequency. The initial antenna was loaded with an L-shaped slot to achieve circular polarization. Multiple rectifying circuits for different bands were designed, fabricated, and tested. The measured results show considerably good output DC voltages. The results also show that conversion efficiencies up to 89% can be achieved.

A highly efficient compact rectenna for wireless energy harvesting at 900 MHz was designed and experimentally evaluated by Ladan *et al.* [59]. This rectenna circuit takes advantage of a compact and light-weight folded dipole antenna connected to a highly efficient rectifier in a doubler voltage structure using HSMS 2862 Schottky diode from Avago technology. To have a higher efficiency, a proper matching network was considered, which could provide the measured efficiency of 60% for 5 mW input power. To decrease the maximum dimensions of the antenna to satisfy the condition of the competition and achieve a high value of FoM, a folded dipole antenna was designed in a square-shaped structure. The measured gain of the antenna was 1.8 dBi at 900 MHz. The rectifier and the antenna were tested individually, and the measurements were in good agreement with the simulation results. Then they were integrated together and fabricated on a single 5880 Rogers substrate and measured as a rectenna. The designed rectenna was able to harvest power from a 900-MHz wireless source located at 1.2 m from the rectenna, which produced about 80 mW/m^2.

Experimental studies on the improvement of the efficiency of a small-sized rectenna using an LC resonator with high-Q characteristics at 950 MHz are presented by Ogawa *et al.* [60]. The developed rectenna features compact dimensions of 20 mm × 13 mm. By choosing an optimum LC combination, an RF-DC conversion efficiency of 85.6% for a 10-mW input power has been attained. Furthermore, at a low-input power of 1 mW and 0.1 mW, RF-DC conversion efficiencies of 73.2% and 40% have been achieved, respectively. Using the developed rectenna, experiments on long distance wireless power transmission were performed, and its ability to transmit power to distant wireless devices in an actual radio wave propagation environment was confirmed.

The design and test of a wearable, multiband ring-antenna together with its rectifying circuit is presented by Masotti and Costanzo [61]. The system is required to harvest RF energy from GSM 900, GSM 1800, and Wi-Fi sources available in the ambience. An annular ring topology is selected for the antenna to be printed on textile and flexible substrates and is suitably modified with appropriate slots to cover the bands of interest. The rectenna efficiency peak has been optimized to correspond to transmitted power levels around 100 mW, which are feasible in the presence of several RF sources.

A 2.45-GHz rectenna using a compact dual circularly polarized (DCP) patch antenna with an RF–DC power conversion part is presented by Harouni *et al.* [62]. The DCP antenna is coupled to a microstrip line by an aperture in the ground plane and includes a bandpass filter for harmonic rejections. It exhibits a measured bandwidth of 2,100 MHz (10 dB return loss) and a 705-MHz CP bandwidth (3 dB axial ratio). The maximum efficiency and DC voltage are, respectively, equal to 63% and 2.82 V over a resistive load of 1,600 Ω for a power density of 0.525 mW/cm^2.

A rectenna is designed by Olgun *et al.* [3] to harvest electrical energy for powering RFIDs from ambient electromagnetic radiation at the 2.45 GHz. The rectenna structure is formed by a Koch fractal patch antenna and a two-stage Dickson charge pump voltage doubling rectifying circuit. The proposed rectenna achieved a good RF–DC conversion efficiency (up to 70%).

A dual-polarized rectenna operating at 2.45 GHz is presented by Vera *et al.* [63]. The antenna consists of a square aperture coupled patch with a cross shaped slot etched on its surface. The received signal from each slot output is rectified by a voltage doubling circuit and DC output signals are combined allowing the rectenna to receive signals of arbitrary polarization. Simulated rectifier maximum RF–DC conversion efficiency values of 15.7% and 42.1% are obtained, respectively, for input available power levels of 20 and 10 dBm, respectively.

Furthermore, wide band and circularly polarized rectennas have been introduced. Hagerty *et al.* [50] presented two rectenna arrays that are suitable for arbitrarily polarized incident waves. The first is a grid array that rectifies two orthogonal linear polarizations, and the second is a spiral array with alternating right-hand and left-hand circular polarizations. The two arrays operate from 4.5 to 8 GHz and 8.5 to 15 GHz and have maximum open circuit voltages of 3.5 and 4 V, respectively. In addition, their efficiencies increase above 35% and 45% for higher incident powers.

6 Conclusion

This chapter provided a review of the most recent wearable antenna designs and applications. It also discussed the electrical characterization of textiles and the methods used to estimate their relative permittivity and loss tangent. The design and analysis of rectifying circuits used in RF energy scavenging was examined with focus on their sensitivity and conversion efficiency. The latest rectenna designs were then surveyed. As the use of wireless devices is blooming, so as the interest in green energy, and due to the limited power that can be generated using RF rectennas, a combination of solar and RF energy harvesting technologies is indeed a direction to consider in the future.

References

[1] Tesla, N., Experiments with alternate currents of high potential and high frequency. *Journal of the Institution of Electrical Engineers*, **21(97)**, pp. 51, 1892.

[2] Brown, W.C., The history of power transmission by radiowaves. *IEEE Transactions on Microwave Theory & Techniques*, **32(9)**, pp. 1230–1242, 1984.

[3] Olgun, U., Chi-Chih, C. & Volakis, J.L., Wireless power harvesting with planar rectennas for 2.45 GHz RFIDs. *Proceedings of International Symposium on Electromagnetic Theory (EMTS 2010)*, Berlin, Germany, pp. 329–331, 2010.

[4] Kim, S., RF energy harvesting techniques for wirelessly powered devices. *IEEE International Microwave Workshop Series on Intelligent Radio for Future Personal Terminals (IMWS-IRFPT 2011)*, Daejeon, Korea, pp. 1–2, 2011.

[5] Merabet, B., Costa, F., Takhedmit, H., Vollaire, C., Allard, B., Cirio, L. & Picon, O., A 2.45-GHz localized elements rectenna. *Proceedings of the 3rd*

IEEE International Symposium on Microwave, Antenna, Propagation and EMC Technologies for Wireless Communications, Beijing, China, pp. 419–422, 2009.

[6] Jabbar, H., Song, Y.S. & Jeong, T.T., RF energy harvesting system and circuits for charging of mobile devices. *IEEE Transactions on Consumer Electronics*, **56(1)**, pp. 247–253, 2010.

[7] Zhang, Z., Vulin, L. & Pan, G., Wide bandwidth measurement of permittivity using multi-resonant modes. *Proceedings of the IEEE 2006 Antennas and Propagation Society International Symposium*, Albuquerque, NM, pp. 1449–1452, 2006.

[8] Rishani, N.R., AI-Husseini, M., EI-Hajj, A. & Kabalan, K.Y., Design and relative permittivity determination of an EBG-based wearable antenna. *Proceedings of the 2012 Progress in Electromagnetics and Radio Frequency (PIERS-2012)*, Moscow, Russia, pp. 96–99, 2012.

[9] Haskou, A., Ramadan, A., Al-Husseini, M., Kasem, F., Kabalan, K.Y. & El-Hajj, A., A simple estimation and verification technique for electrical characterization of textiles. *Proceedings of the 2012 Middle East Conference on Antennas and Propagation (MECAP 2012)*, Cairo, Egypt, pp. 1–4, 2012.

[10] Declercq, F., Couckuyt, I., Rogier, H. & Dhaene, T., Complex permittivity characterization of textile materials by means of surrogate modelling. *Proceedings of the 2010 IEEE Antennas and Propagation Society International Symposium (APSURSI 2010)*, Toronto, Canada, pp. 1–4, 2010.

[11] Lee, M.-Q. & Nam, S., An accurate broadband measurement of substrate dielectric constant. *IEEE Microwave Guided Wave Letter*, **6**, pp. 168–170, 1996.

[12] Cottet, D., Gryzb, J., Kirstein, T. & Tröster, G., Electrical characterization of textile transmission lines. *IEEE Transactions on Advanced Packaging*, **26**, pp. 182–190, 2003.

[13] Declercq, F. & Rogier, H., Characterization of electromagnetic properties of textile materials for the use in wearable antennas. *Proceedings of the 2009 IEEE International Symposium on Antennas and Propagation Society (APSURSI 2009)*, Charleston, NC, pp. 1–4, 2009.

[14] Rishani, N., Circularly polarized wearable antenna with EBG for GPS applications. Master Thesis, American University of Beirut, 2011.

[15] Delcotex Germany, www.delcotex.de

[16] Declercq, F., Couckuyt, I., Rogier, H. & Dhaene, T., Environmental high frequency characterization of fabrics based on a novel surrogate modelling antenna technique. IEEE Transactions on *Antennas and Propagation*, **61(10)**, pp. 5200–5213, 2013.

[17] Nagy, L. & Szalay, Z., Coaxial resonator and measuring system for dielectric parameter measurements. Proceedings of the *6th European Conference on Antennas and Propagation (EUCAP 2012)*, Prague, Czech Republic, pp. 2149–2153, 2012.

[18] Szalay, Z., Ther, I. & Nagy, L., Complex dielectric parameter measurement by coaxial resonator and ISM band radio module. *Proceedings of t*he *23rd*

International Conference Radioelektronika (RADIOELEKTRONIKA 2013), Pardubice, Czech Republic, pp. 213–218, 2013.

[19] Kehn, M.N.M., Shafai, L. & Noghanian, S., Permittivity measurement of disk and annular dielectric samples using coaxial transmission line fixtures. Part I: Theory and formulation. Canadian Journal of *Electrical and Computer Engineering*, **34(1/2)**, pp. 21–29, 2009.

[20] Kehn, M.N.M., Shafai, L., Safari, F. & Noghanian, S., Permittivity measurement of disk and annular dielectric samples using coaxial transmission line fixtures. Part II: experimentation and accuracy analyses. *Canadian Journal of Electrical and Computer Engineering*, **34(1/2)**, pp. 31–41, 2009.

[21] Declercq, F., Rogier, H. & Hertleer, C., Permittivity and loss tangent characterization for garment antennas based on a new matrix-pencil two-line method. IEEE Transactions on *Antennas and Propagation*, **56(8)**, pp. 2548–2554, 2008.

[22] Nepa, P. & Manara, G., Design and characterization of wearable antennas. *Proceedings of the 2013 International Conference on Electromagnetics in Advanced Applications (ICEAA 2013)*, Torino, Italy, pp. 1168–1171, 2013.

[23] Monti, G., Corchia, L. & Tarricone, L., UHF wearable rectenna on textile materials. *IEEE Transactions on Antennas and Propagation*, **61(7)**, pp. 3869–3873, 2013.

[24] Rais, N.H.M., Soh, P.J., Malek, F., Ahmad, S., Hashim, N.B.M. & Hall, P.S., A review of wearable antenna. *Proceedings of the 2009 Loughborough Antennas & Propagation Conference (LAPC 2009)*, Loughborough, UK, pp. 225–228, 2009.

[25] Osman, M.A.R., Abd Rahim, M.K., Samsuri, N.A., Salim, H.A.M. & Ali, M.F., Embroidered fully textile wearable antenna for medical monitoring applications. *Progress in Electromagnetics Research*, **117**, pp. 321–337, 2011.

[26] Khaleel, H.R., Al-Rizzo, H.M., Rucker, D.G. & Elwi, T.A., Wearable Yagi microstrip antenna for telemedicine applications. *Proceedings of the 2010 IEEE Radio and Wireless Symposium (RWS 2010)*, New Orleans, LA, pp. 280–283, 2010.

[27] Fletcher, R.R. & Kulkarni, S., Wearable Doppler radar with integrated antenna for patient vital sign monitoring. *Proceedings of the 2010 IEEE Radio and Wireless Symposium (RWS 2010)*, New Orleans, LA, pp. 276–279, 2010.

[28] Reina-Tosina, J., Roa, L.M. & Prado, M., Design of antennas for a wearable sensor for homecare movement monitoring. *Proceedings of the 28th Annual International Conference of the IEEE Engineering in Medicine and Biology Society (EMBS 2006)*, New York, NY, pp. 5972–5976, 2006.

[29] Mandal, S., Turicchia, L. & Sarpeshkar, R., A low-power, battery-free tag for body sensor networks. *IEEE Pervasive Computing*, **9(1)**, pp. 71–77, 2010.

[30] Wang, Y., Li, L., Wang, B. & Wang, L., A body sensor network platform for in-home health monitoring application. *Proceedings of the 4th International Conference on Ubiquitous Information Technologies Applications (ICUT 2009)*, Fukuoka, Japan, pp. 1–5, 2009.

[31] Zhang, T.T. & Ser, W., Mutual coupling effect of antenna array communications systems for portable medical devices. *Proceedings of the 4th IEEE International Conference on Industrial Electronics and Applications (ICIEA 2009)*, Fukuoka, Japan, pp. 549–553, 2009.

[32] Carmo, J.P., Dias, N., Mendes, P.M., Couto, C. & Correia, J.H., Low-power 2.4-GHz RF transceiver for wireless EEG module plug-and-play. *Proceedings of the 13th IEEE International Conference on Electronics, Circuits and Systems (ICECS 2006)*, Nice, France, pp. 1144–1147, 2006.

[33] Lilja, J. & Salonen, P., Textile material characterization for softwear antennas. *Proceedings of the 2009 IEEE Military Communications Conference (MILCOM 2009)*, Boston, MA, pp. 1–7, 2009.

[34] Vallozzi, L., Rogier, H. & Hertleer, C., Dual polarized textile patch antenna for integration into protective garments. *IEEE Antennas and Wireless Propagation Letters*, 7, pp. 440–443, 2008.

[35] Vallozzi, L., Van Torre, P., Hertleer, C., Rogier, H., Moeneclaey, M. & Verhaevert, J., Wireless communication for firefighters using dual-polarized textile antennas integrated in their garment. *IEEE Transactions on Antennas and Propagation*, **58(4)**, pp. 1357–1368, 2010.

[36] Tillery, J.K., Thompson, G.T. & Wang, J.J.H., Low-power IOW-profile multifunction helmet-mounted smart array antenna. *Proceedings of the 1999 IEEE Antennas and Propagation Society International Symposium (APSURSI '09)*, Charleston, SC, pp. 1554–1557, 1999.

[37] Cibin, C., Leuchtmann, P., Gimersky, M., Vahldieck, R. & Moscibroda, S., A flexible wearable antenna. *Proceedings of the 2004 IEEE Antennas and Propagation Society International Sym*posium, Sendai, Japan, pp. 3589–3592, 2004.

[38] Sanz-Izquierdo, B., Huang, F. & Batchelor, J.C., Small size wearable button antenna. *Proceedings of the First European Conference on Antennas and Propagation (EuCAP 2006)*, Nice, France, pp. 1–4, 2006.

[39] Sanz-Izquierdo, B. & Batchelor, J.C., A dual band belt antenna. *Proceedings of the 2008 International Workshop on Antenna Technology: Small Antennas and Novel Metamaterial (iWAT*2008), Chiba, Japan, pp. 374–377, 2008.

[40] Salonen, P., Keskilammi, M. & Sydanheimo, L., Antenna design for wearable applications. *Proceedings of the 2001 World Multiconference on Systemics, Cybernetics, and Informatics*, Orlando, FL, pp. 496–502, 2001.

[41] Yilmaz, E., Kasilingam, D.P. & Notaros, B.M., Performance analysis of wearable microstrip antennas with low-conductivity materials. *Proceedings of the 2008 IEEE Antennas and Propagation Society International Symposium (AP-S 2008)*, San Diego, CA, pp. 1–4, 2008.

[42] Chahat, N., Zhadobov, M. & Sauleau, R., Yagi-Uda textile antenna for on-body communications at 60 GHz. *Proceedings of the 7th European Conference on Antennas and Propagation (EuCAP 2013)*, Gothenburg, Sweden, pp. 411–413, 2013.

[43] Chahat, N., Zhadobov, M., Muhammad, S.A., Le Coq, L. & Sauleau, R., 60-GHz textile antenna array for body-centric communications. *IEEE Transactions on Antennas and Propagation*, **61(4)**, pp. 1816–1824, April 2013.

[44] Castel, T., Van Torre, P., Tanghe, E., Agneennens, S., Vermeeren, G., Joseph, W. and Rogier, H., Improved reception of in-body signals by means of a wearable multi-antenna system. *International Journal of Antennas and Propagation*, **2013**, pp. 1–9, 2013, article ID 328375.

[45] Lui, K.W., Murphy, O.H. & Toumazou, C., A wearable wideband circularly polarized textile antenna for effective power transmission on a wirelessly-powered sensor platform. *IEEE Transactions on Antennas and Propagation*, **61(7),** pp. 3873–3876, 2013.

[46] Haskou, A., Design of wearable rectennas for RF energy harvesting. Master Thesis, American University of Beirut, April 2013.

[47] Zhu, S. & Langley, R., Dual-band wearable textile antenna on an EBG substrate. *IEEE Transactions on Antennas and Propagation*, **57(4)**, pp. 926–935, 2009.

[48] Khaleel, H.R., Abbosh, A.I., Al-Rizzo, H.M., & Rucker, D.G., Flexible and compact AMC based antenna for telemedicine applications. *IEEE Transactions on Antennas and Propagation*, **61(2)**, pp. 524–531, 2013.

[49] Marian, V., Vollaire, C., Allard, B. & Verdier, J., Low power rectenna topologies for medium range wireless energy Transfer. *Proceedings of the 14th European Conference on Power Electronics and Applications (EPE2011)*, Birmingham, UK, pp. 1–10, 2011.

[50] Hagerty, J.A., Lopez, N.D., Popovic, B. & Popovic, Z., Broadband rectenna arrays for randomly polarized incident waves. *Proceedings of 30th European Microwave Conference (EUMC 2010)*, Paris, France, pp. 1–4, 2010.

[51] Taris, T., Vigneras, V. & Fadel, L., A 900 MHz RF energy harvesting module. Proceedings of the *IEEE 10th International New Circuits and Systems Conference (NEWCAS2012)*, Montreal, Canada, pp. 445–448, 2012.

[52] Olgun, U., Chi-Chih, C. & Volakis, J.L., Investigation of rectenna array configurations for enhanced RF power harvesting. *IEEE Antennas and Wireless Propagation Letters*, **10**, pp. 262–265, 2011.

[53] Muramatsu, M. & Koizumi, H., An experimental result using RF energy harvesting circuit with Dickson charge pump. *IEEE International Conference on Sustainable Energy Technologies (ICSET)*, Kandy, Sri Lanka, pp. 1–4, 2010.

[54] Devi, K.K.A., Norashidah, M.D., Chakrabarty, C.K. & Sadasivam, S., Design of an RF-DC conversion circuit for energy harvesting. *IEEE International Conference on Electronics Design, Systems and Applications (ICEDSA)*, Kuala Lumpur, Malaysia, pp. 156–161, 2012.

[55] Arrawatia, M., Baghini, M.S. & Kumar, G., RF energy harvesting system at 2.67 and 5.8 GHz. *Proceedings of the 2010 Asia-Pacific Microwave Conference (APMC 2010)*, Yokohama, Japan, pp. 900–903, 2010.

[56] Karolak, D., Taris, T., Deval, Y., Begueret, J.B. & Mariano, A., Design comparison of low-power rectifiers dedicated to RF energy harvesting.

Proceedings of the 19th IEEE International Conference on Electronics, Circuits and Systems (ICECS 2012), Seville, Spain, pp. 524–527, 2012.

[57] Hao, G., Matters-Kammerer, M.K., Harpe, P., Milosevic, D., Johannsen, U., Van Roermund, A. & Baltus, P., A 71 GHz RF energy harvesting tag with 8% efficiency for wireless temperature sensors in 65nm CMOS. *Proceedings of the IEEE Radio Frequency Integrated Circuits Symposium (RFIC)*, Seattle, WA, pp. 403–406, 2013.

[58] Huyen, L., Fong, N. & Luong, H.C., RF energy harvesting circuit with on-chip antenna for biomedical applications. *Proceedings of the Third International Conference on Communications and Electronics (ICCE 2010)*, NhaTrang, Vietnam, pp. 115–117, 2010.

[59] Ladan, S., Ghassemi, N., Ghiotto, A. & Wu, K., Highly efficient compact rectenna for wireless energy harvesting application. *IEEE Microwave Magazine*, **14(1)**, pp. 117–122, 2013.

[60] Ogawa, K., Ozaki, K., Yamada, M. & Honda, K., High efficiency small-sized rectenna using a high-Q LC resonator for long distance WPT at 950 MHz. *IMWS-IWPT 2012*, Kyoto, 2012.

[61] Masotti, D. & Costanzo, A., Design of wearable rectennas harvesting from multi-tone ambient RF sources. *Proceedings of the* 4th International. Symposium on Applied Sciences in Biomedical and Communication Technologies, Barcelona, Spain, pp. 1–4, 2011.

[62] Harouni, Z., Cirio, L., Osman, L., Gharsallah, A. & Picon, O., A dual circularly polarized 2.45-GHz rectenna for wireless power transmission. *IEEE Antennas and Wireless Propagation Letters*, **10**, pp. 306–309, 2011.

[63] Vera, G.A., Georgiadis, A., Collado, A. & Via, S., Design of a 2.45 GHz rectenna for electromagnetic (EM) energy scavenging. *Proceedings of the 2010 IEEE Radio and Wireless Symposium (RWS 2010)*, New Orleans, LA, pp. 61–64, 2010.